Research Article

Optimization of ATP System Based on Quantum Secure Communication and Its Tracking Control Strategy

Jin Liu,[1] Fan Zhang,[1] Carlo Cattani [ID],[2] Haima Yang [ID],[3] and Song Wanqing[1]

[1]*School of Electronic and Electrical Engineering, Shanghai University of Engineering Science, Shanghai 201620, China*
[2]*Engineering School, DEIM University of Tuscia, Viterbo 1100, Italy*
[3]*School of Optical-Electrical and Computer Engineering, University of Shanghai for Science and Technology, Shanghai 200093, China*

Correspondence should be addressed to Carlo Cattani; cattani@unitus.it and Haima Yang; snowyhm@sina.com

In quantum key distribution experiments, ground motion is usually used to simulate satellite-based motion. The posture fluctuation of the platform affects the normal operation of the acquisition, tracking, and pointing (abbreviated as ATP) system seriously. To achieve the verification of the ground motion platform, the ATP parameters of the ground simulation motion system cannot be designed only according to the satellite-based ATP parameters. To solve this problem, a set of initial pointing system and inertial stabilization system is added to the simulation ATP system. This provides a technical solution for the ground simulation ATP system similar to the satellite-based motion platform. In the meanwhile, a tracking control strategy based on the identification method is proposed by establishing identification symbols. Compared with traditional proportion, integral, and differential (abbreviated as PID) control, this method overcomes the shortcoming of tentative modification of the control parameters and improves the stability and adaptability of the tracking control process. Tracking accuracy of ±0.1° is achieved under heavy-load conditions. This guarantees the success of the quantum key distribution (QKD) verification test of the ground motion platform.

1. Introduction

In an ATP system, one party of the communication link sends a wide beam of beacon light for scanning, and the other party searches for the beacon light [1]. After the beacon light enters the detector field and is detected correctly, the end units on both sides control the tracking mechanism based on the visual axis deviation provided by the detector so that its boresight follows the visual axis of the incident light [2, 3]. After the double-ended visual axis points to the other's visual axis correctly, it indicates that the optical communication link has been established and the communication process can start. Laser aiming, tracking, and capturing are the important parameters of the exact alignment of the terminal equipment for spatial optical communication [4]. The technical parameters of the traditional ATP system are designed purely according to the satellite-based ATP parameters, and innovative improvements have not been made

because the laser beam passes through the atmosphere and air during transmission; the geometric attenuation will occur in this process [5, 6]. Besides, the transmission distance is long because the original ATP system in the quantum key distribution has insufficiently tracking bandwidth on the motion platform and the target acquisition time is long. It is difficult to verify the ground motion platform [7]. The traditional ATP system cannot achieve high control precision and bandwidth, so the capturing probability of the ATP system has been reduced and the capturing time has been increased. Therefore, improving the tracking accuracy and tracking bandwidth are the key technologies that are necessary to solve in intersatellite optical communication [8].

To solve these problems which have been mentioned, the free-space quantum key distribution experiment is carried out on different motion platforms, and the motion platform is tested in this paper. The motion characteristics of the vehicle motion platform, the hot-air balloon motion

platform, and the airborne motion platform are analyzed. The primary tracking section has been added to improve the efficiency and stability of capturing, tracking, and targeting. In the tracking strategy, the symbol method control is introduced, and different control strategies are generated by different symbol vectors [9, 10]. Thus, a stable and adaptive target tracking control process is achieved, and the shortcoming of modifying the control parameters tentatively in the original PID control method can be overcome.

2. Beacon Initial Pointing System

The beacon initial pointing system plays an important role in the QKD ground verification experiment, as shown in Figure 1. For satellite-based motion platforms, ATP data is the attitude stabilization parameter that could be provided by the Earth observation satellite platform. From the technical indicators, the satellite platform is an excellent platform with good stability. However, it is difficult for the motion platform to simulate good attitude stability in the actual field.

Structural problems, solar panels, inertial flywheels, and antenna pointing mechanisms can cause 0–200 Hz vibration in the satellites. Among them, the main vibration zone is within 1 Hz, which is mainly generated by solar windsurfing, equivalent to a pointing vibration of 100 μrad in the pointing mechanism. Due to the action of the inertia flywheel, a 100 Hz vibration is generated, which is equivalent to a pointing vibration of 4 μrad in the pointing mechanism. The inertia flywheel also produces a second harmonic vibration of 200 Hz, equivalent to a pointing vibration of 0.6 μrad in the pointing mechanism [11].

2.1. Initial Pointing Turntable.
In the QKD experiment, the ground station needs to use the turntable with a large-load motor to complete the initial pointing function of the receiving Bob end. The initial pointing installation structure is shown in Figure 2. Due to the quality of the ground station, Bob is 150 kg, the drive control system has higher requirements for the bearing capacity of the turntable. By the table driven by the stepper motor, the following technical requirements can be met: driving load is 150 kg, running speed is 0~10°/s, running acceleration is 2°/s^2, table vibration is less than 0.01 mm, and repeat positioning accuracy is 0.002°. The drive motor is a three-phase hybrid stepping motor with a worm gear reduction ratio of 180 : 1 and a backlash of 0.05°. When commutation is frequent, the soft connection of the table has a certain stiffness to shock absorption, thereby the high-frequency vibration caused by the gap within the turntable is isolated.

2.2. Inertial Stabilization Platform.
Since the sender, Alice, needs to be installed on the platform to move, but the platform itself has a strong posture fluctuation, it needs to be isolated. A stable attitude close to the satellite-based motion platform (in fact, far worse than the star-based motion platform) is provided. Leica's PAV30 inertial stabilization platform is used as the damping platform. The installation structure is shown in Figure 3.
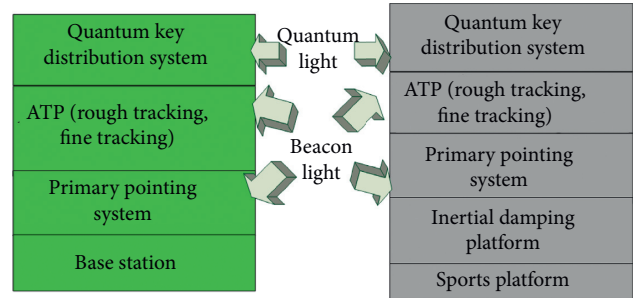

FIGURE 1: Three-level pointing system.
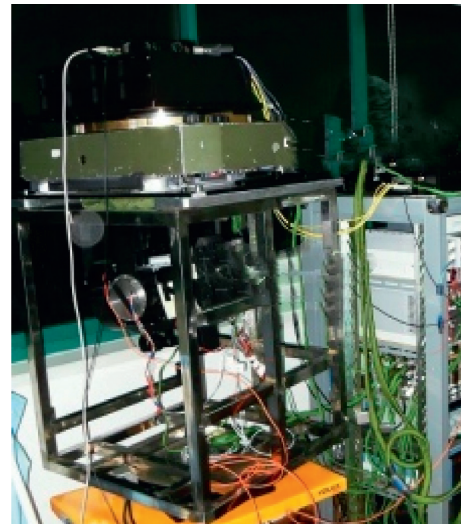

FIGURE 2: Large-load motor turntable.

FIGURE 3: Inertial stabilization platform.

The PAV30 is an excellent inertial stability platform that isolates high-frequency oscillations in the pitch and roll directions of the motion platform [12]. The internal structure of the PAV30 consists of three control loops: the azimuth loop, the pitch loop, and the rolling loop. The azimuth loop can be used for orientation control when the navigation

component is externally connected, or it can be controlled by an external processor through the handle. The pitch loop and the rolling loop are self-leveling inertial control via a built-in rate gyro. The internal servo motor is a DC torque motor, and the three-loop motion is controlled by the wire rope pulling method. It has good shock absorption and stability characteristics [13–15]. In the technical specifications of the PAV30, the pitch and roll angle control range are 5°, the azimuth angle control range is ±30°, and the external vibration suppression capability is shown in Figure 4.

It could be seen from Figure 4, the external vibration frequency is higher than 10 Hz. It will be suppressed to 1% in the inertial stabilization platform and then it can provide a stable inertial and attitude mounting area in the inner loop.

3. Characteristics of the Motion Platform

3.1. Vehicle Motion Platform. In the long-distance atmospheric environment, to test the ATP characteristics of the ground station Bob and the transmitting end Alice and to verify the influence of atmospheric turbulence and the vehicle motion platform on the actual tracking performance, a 32 km vehicle-mounted tracking experiment is carried out. As the equipment is relatively large and heavy, the transmitter Alice is installed on the pickup truck. The installation structure of the vehicle motion platform is shown in Figure 5. The ASV940P attitude sensor which is installed into the trunk with a damping cushion is used to measure the motion characteristics of the vehicle. Test data is shown in Figures 6(a) and 6(b) and Figures 7(a) and 7(b).

It can be seen from Figures 6(a) and 6(b) and Figures 7(a) and 7(b) that the vibration component of the vehicle vibration spectrum at 3–20 Hz is significantly increased in the pitch and roll directions before and after the vehicle is started. The broadening of the vibration spectrum in the rolling direction is greater than that in the pitch direction. In the four-wheel alignment of the vehicle body, the front and rear track distances are greater than that of the left and right wheel tracks, so that the stability of the pitch direction is greater than that of the roll direction. The movement characteristics of the vehicle such as going straight, passing through the bridge, and turning are shown in Figure 8.

In Figure 8, the vehicle passes through a straight road at a max speed of 60 km/h, and there are two bridges on the road. Segment 1 indicates passing through bridge 1. Segment 2 indicates avoiding obstacles on the road. Segment 3 indicates passing through bridge 2, and segment 4 indicates turning back. The angle of the two bridges is from 3 to 5 degrees. It can be seen from the attitude curve that the fluctuation of the road surface affects the attitude data of the vehicle's pitch and roll directions seriously. The maximum angular change in the pitch direction is close to 15° and the rate of change is 3°/s. The maximum angular change in the roll direction is close to 10° and the rate of change is 5°/s. These changes are highly dependent on the condition of the road and the speed of driving. Therefore, the posture of the vehicle motion platform is subject to the shape of the road surface, the traveling speed, the driving habits of the driver, and proficiency. It is necessary to consider the isolation platform and the slow operation.
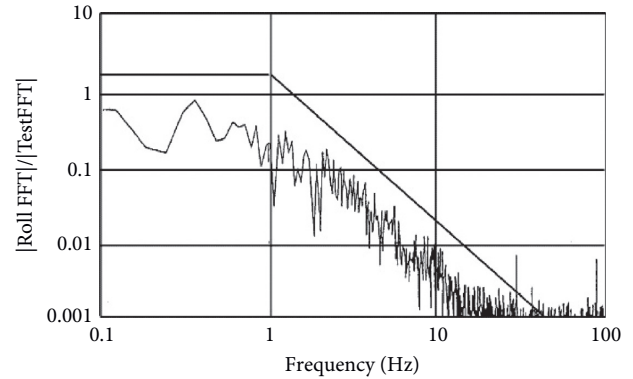

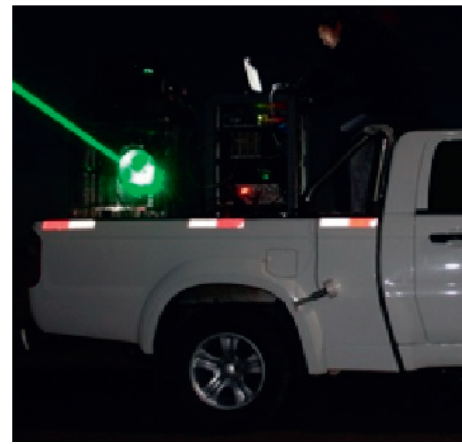Figure 4: PAV30 rolling dynamic suppression spectrum.

Figure 5: Car sports' platform settings.

3.2. Hot-Air Balloon Motion Platform. The hot-air balloon platform is manufactured by Nanjing Hongguang Special Equipment Factory. The basic technical parameters of the hot-air balloon are as follows: balloon volume is 4000 m³, ball height is 24 m, sphere diameter is 19 m, take-off weight is 900 kg, net load is 600 kg, average rising speed is 2.8 m/s, and tie-in time is 2 hours (depending on weather environment). The Ellipse-N attitude sensor installed into the hanging basket is used to measure the motion characteristics of the hot-air balloon. Since the hot-air balloon float experiment is subject to weather conditions and airspace management requirements, only tethered flight mode can be used during night experiments. There are two tie ropes and each rope is 150 m. The lift range of the air balloon is more than 100 m, and the tethered flight experiment requires an ambient wind speed <3 m/s. Otherwise, the release of hot-air balloons will be greatly affected by atmospheric disturbances, the motion posture will be disordered, and it is dangerous. The installation of the hot-air balloon motion platform is a large hanging basket form, and Alice is installed into the large hanging basket. Figure 9 shows the fixing and installation of the hanging basket. The data is shown in Figures 10(a) and 10(b)–Figures 12(a) and 12(b). The test conditions are as follows: wind speed 2.7 m/s, mooring flight, and average flight height 15 m.
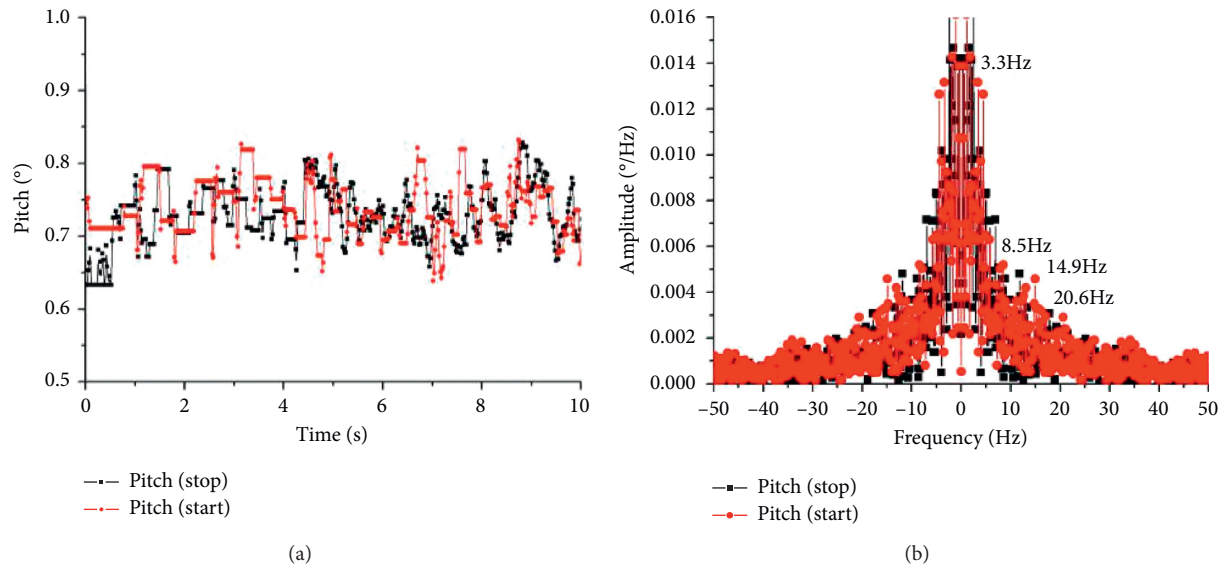
(a)

(b)

Figure 6: (a) Pitch angle change when the engine starts and stops. (b) Pitch spectrum change when the engine starts and stops.
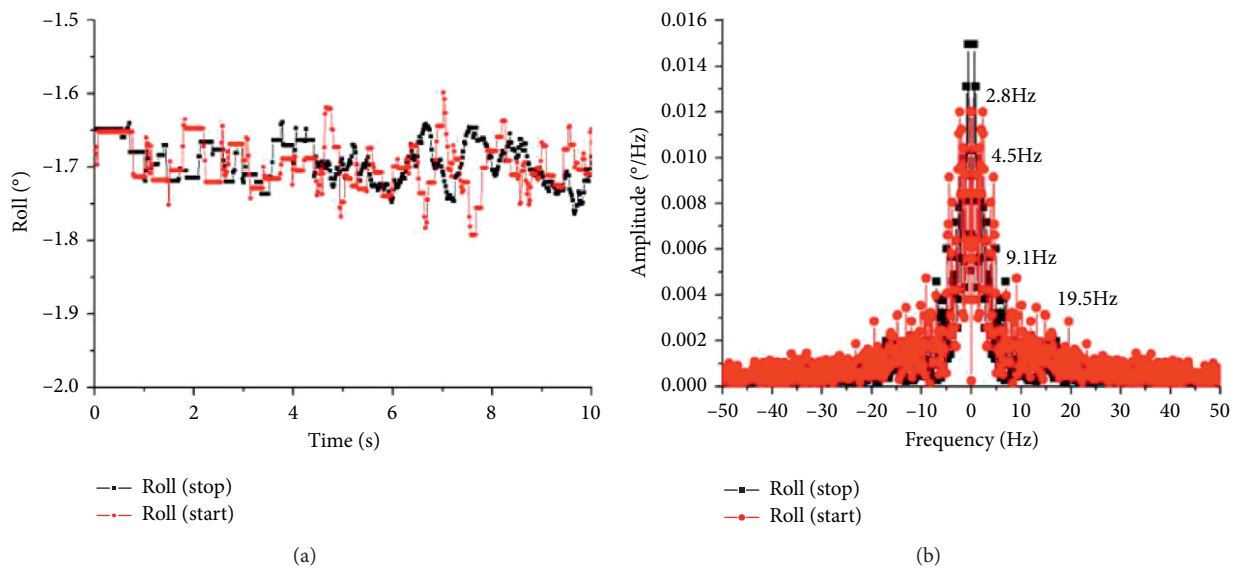

(a)

(b)

Figure 7: (a) Rolling angle change when the engine starts and stops. (b) Fluke spectrum change when the engine starts and stops.

From Figures 10(a) and 10(b)–Figures 12(a) and 12(b), it could be seen that there is a natural frequency of free swing in the azimuth angle of the attitude of the hot-air balloon due to its inertia and the external force of the mooring rope. The frequency component in the pitch and roll directions is 0.06 Hz. In addition to this, there is a frequency component of 0.35 Hz. The frequency component should be caused by atmospheric turbulence and ignition vibration of the flame ejector (to keep the balloon height stable, the ignition frequency of the flame ejector is about 3 seconds per time). In a hot-air balloon, when an inertial stabilization platform is installed, the attitude suppression curve of the pitch direction in the platform is shown in Figure 13. The measurement data of Figure 13 comes from the attitude sensor, and the data in the inertial platform comes from the

photoelectric position tracking sensor (2D-PSD detector) which is used for initial pointing.

As it can be seen from Figure 13, the inertial stabilization platform of the hot-air balloon suppresses the fluctuation of the external pitch direction. In the meanwhile, the angle change of the pitch of the hanging basket is controlled within ±3°, and the angle change of the pitch in the stable inertial platform is controlled within ±0.5°.

3.3. Airborne Motion Platform. The helicopter platform can be used to serve the airborne motion platform. Because the helicopter's air attitude control is convenient, it can hover in the air. The helicopter platform in this experiment is a Z-9 model. The helicopter hovers in the air and the attitude sensor is mounted on the inner deck of the cabin. During the
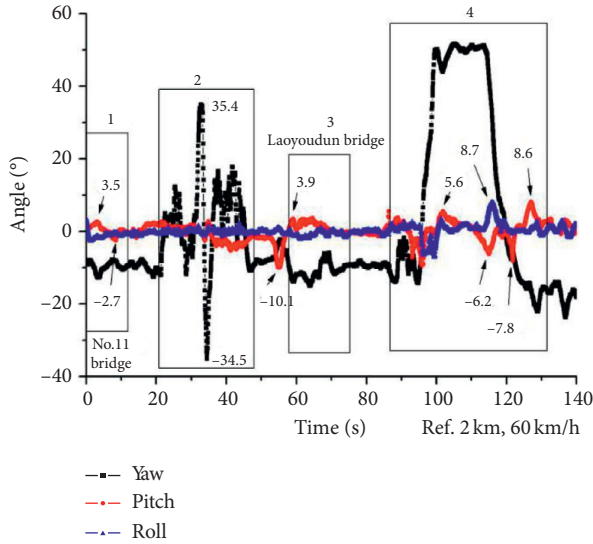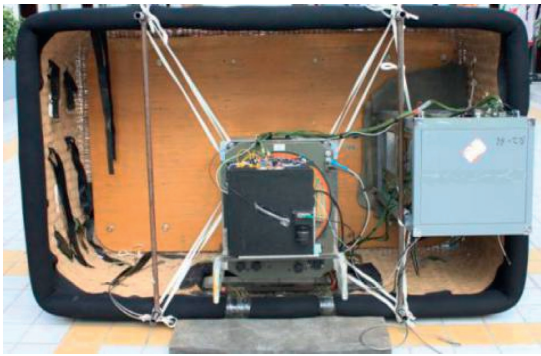
FIGURE 8: The running posture of the vehicle.

FIGURE 9: Hot-air balloon large hanging basket installation method.

flight experiment, the flight height of the helicopter is less than 1 km and the flight speed is less than 50 m/s. The flight area has a total length of 10 km from north to south and the flight time is about 20 minutes. The hovering altitude is about 800 meters, the shortest distance between the ground station Bob and the flight route is 2.5 km, and the equivalent maximum overtravel angular velocity is 1.2°/s. The airborne motion platform and mounting structure are shown in Figure 14. The measured flight attitude data are shown in Figures 15(a) and 15(b)–Figures 17(a) and 17(b).

From the data of Figures 15(a) and 15(b)–Figures 17(a) and 17(b), it can be seen that when the helicopter is hovering, the range of helicopter azimuth attitude angle fluctuation is controlled to be smaller than that of a hot-air balloon floating fluctuation range of the azimuth angle. However, the azimuth fluctuation range is still within ±4°, and there is a certain angular drift with time. The range of pitch and roll angles is similar to the two attitude angles of the hot-air balloon. From a spectrum perspective, the high-frequency component is more intense than the hot-air balloon when the helicopter is hovering. There is a strong component at 0–4 Hz, especially at 1.37 Hz, 2.61 Hz with several frequency enhancement points.

4. Identification Control Method in the Initial Direction

When the quantum key QKD experiment is performed, the platform is in motion. The ATP tracking process on both sides is briefly described as follows:

(1) The receiving end Bob turns on the uplink beacon light, and the GPS coordinates sent by the radio station are quickly pointed to Alice according to the GPS pointing algorithm. At the same time, Alice turns on the downlink beacon light, calculates the direction of the beacon light according to the position of Bob, and drives the downlink beacon light to Bob.

(2) The receiving end Bob searches for the downlink beacon light sent by Alice.

(3) When the receiving ends, Bob searches for Alice downlink beacon light, and the uplink beacon light also points to Alice.

(4) After the sender Alice searches for Bob's uplink beacon light, the ATP tracking process is performed.

(5) After the tracking is stable, the quantum key distribution system is turned on.

(6) Quantum key distribution.

(7) If the beacon light is out of target during communication, (1) is repeated.

(8) The distribution of the quantum key is over.

(9) The sender Alice and the receiver Bob turn off the beacon light and reset.

When ground station Bob performs initial pointing tracking, the tracking method is performed by a combination of fuzzy control and improved PID tracking method. The core of the improved control process is a control strategy based on the identification method. The initial pointing structure of the ground station Bob is shown in Figure 18. At the bottom, the large turntable is used for test tracking performance. It does not contain a large turntable structure when the actual outfield is used.

4.1. Initial Conditions and Identification Method. When the identification method control is performed, it is necessary to analyze the controlled object first. It needs to establish an identification feature model of the input signal [16, 17]. For the initial pointing system, the output pulse number F_n of the stepping motor, the motor pulse sending time T_n, and the angle signal collecting time t_n can be controlled. The data that can be collected is the angle array $\phi_n[\theta_1, \ldots, \theta_9, \theta_{\text{Now}}]$ of the target and the array $\psi_n[\beta_1, \ldots, \beta_9, \beta_{\text{Now}}]$ of the angle that points to the system.

The absolute angular coordinate system is established according to the initial direction. Only considering the absolute angular coordinates of the azimuth, which is positive for clockwise and negative for counterclockwise. All angle values are determined by the starting zero points. According to the GPS pointing algorithm, the target is pulled
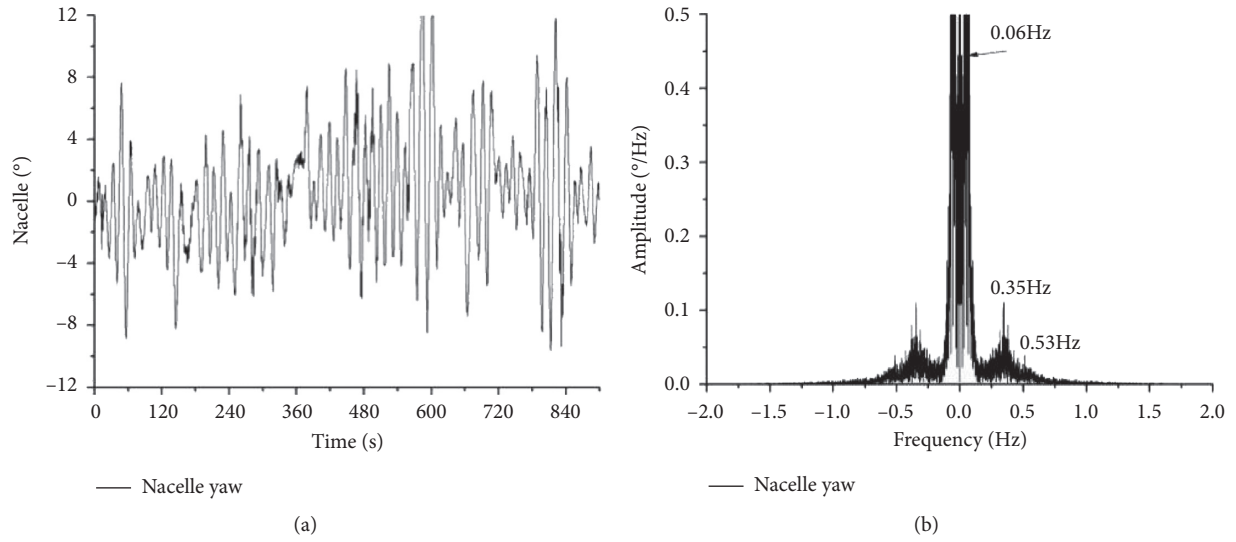
FIGURE 10: (a) Atomic change of hot-air balloon basket. (b) Hot-air balloon basket azimuth spectrum change.
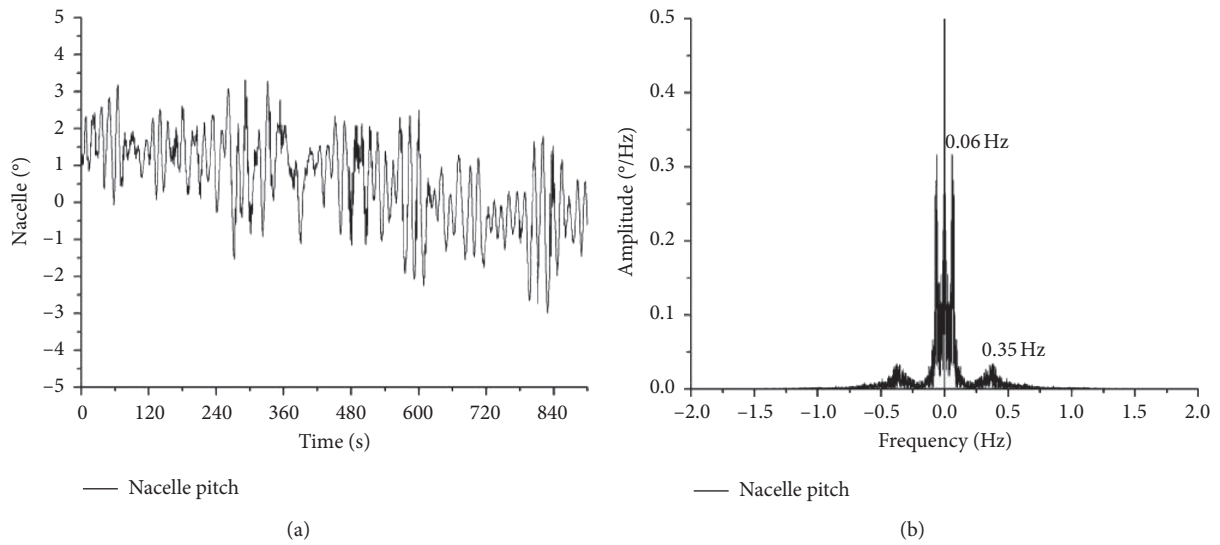

FIGURE 11: (a) Hot-air balloon basket pitch angle change. (b) Hot-air balloon basket pitch spectrum change.
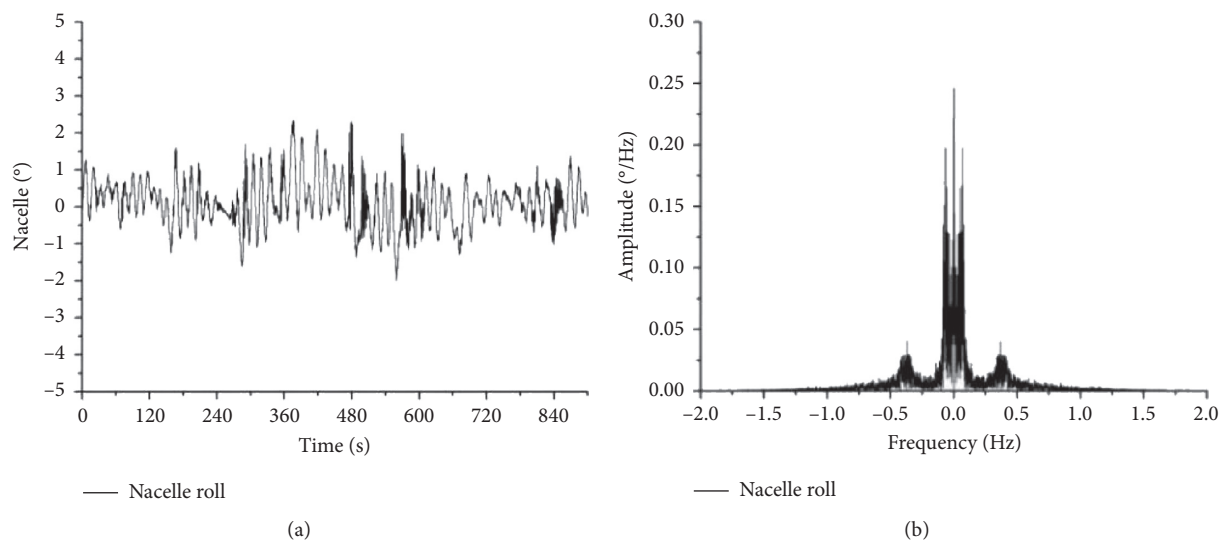

FIGURE 12: (a) The roll angle change of hot-air balloon basket. (b) The rolling spectrum change of hot-air balloon basket.
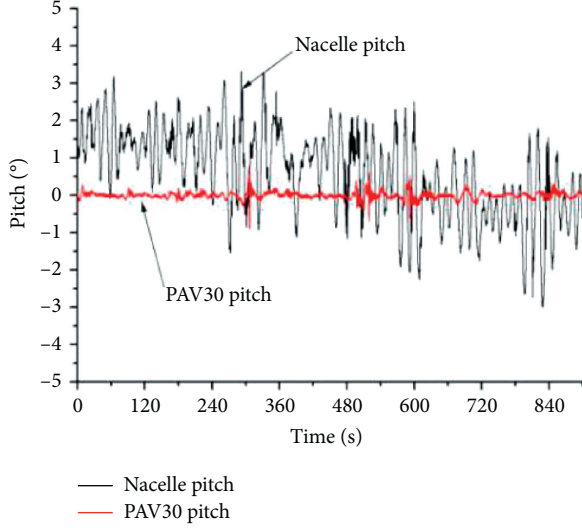
FIGURE 13: Damping performance of inertial stability platform.

FIGURE 14: Setting of the airborne motion platform.

into the field of view of the initial pointing photoelectric tracking position sensor, and then the initial pointing the tracking process begins. Assuming that the initial target is already within the field of view of the two-dimensional photoelectric tracking position sensor, the relationship of the target with time is shown in Figure 19. In this control, $T_n - T_{n-1} = 100\,\text{ms}$, $t_n - t_{n-1} = 10\,\text{ms}$. This is the interval value of two control times, which can also be understood as the data sampling period. F_n is the number of pulses to be emitted within 0.1 s at the nth time. If there is no out-of-synchronization, F_{max} is the maximum number of pulses that the stepper motor is allowed to emit within 0.1 s. The target angle array is ϕ_n, which is the 10 target angle values collected before the current time collected at the time T_n. In general, the ϕ_n array retains the three groups of the most recent time. The angle array of the initial pointing system is ψ_n, which is the value of the 10 initial pointing angles collected before the current time collected at the time T_n. Given by the photoelectric encoder, the general case ψ_n array retains the three groups of the most recent time. There is also a target angle threshold θ_Δ and the number of leading pulses F_Δ that need to be used.

In the initial pointing system, θ_{min} is a pulse corresponding to a stepping angle of the stepper motor. The

overshoot of the tracking target angle is σ_P. Construct the identification quantity Mod.A_n, Mod.B_n, Mod.C_n, Mod.D_n, and establish the symbol operation, which can be expressed as

$$\text{Sign}\,(f_1, f_2, \Delta) = \begin{cases} +, & f_1 - f_2 \geq \Delta, \\ 0, & \text{others}, \\ -, & f_1 - f_2 \leq -\Delta, \end{cases} \quad (1)$$

where Δ is the threshold. The explanation for equation (1) is as follows: formula (1) is equivalent to a reference formula template and does not represent a special meaning. The following construction and symbolic quantities Mod.A_n, Mod.B_n, Mod.C_n, and Mod.D_n are all given in the form of equation (1). For example, f_1 the following formula corresponds to ψ_n, $f2$ and corresponds to ϕ_n.

The target angle deviation symbol Mod.A_n can be expressed as

$$\text{Mod} \cdot A_n = \text{Sign}\,(\psi_n, \phi_n, \theta_\Delta)$$

$$= \begin{cases} +, & \psi_n - \phi_n \geq \theta_\Delta \,(\text{Advance}), \\ 0, & \text{Others (Keep up with)}, \\ -, & \psi_n - \phi_n \leq -\theta_\Delta \,(\text{Lag}), \end{cases} \quad (2)$$

$$\psi_n - \phi_n = \frac{1}{N} \sum_{i=1}^{N} (\beta_i - \theta_i), \quad N = 9. \quad (3)$$

The target motion symbol Mod.B_n can be expressed as

$$\text{Mod} \cdot B_n = \text{Sign}\,(\phi_n, \phi_{n-k}, \theta'_\Delta)$$

$$= \begin{cases} +, & \phi_n - \phi_{n-k} \geq \theta'_\Delta \,(\text{Positive}), \\ 0, & \text{Others}\,(\text{Stop}, k = l \text{ or } 2), \\ -, & \phi_n - \phi_{n-k} \leq -\theta'_\Delta \,(\text{Reverse}), \end{cases} \quad (4)$$

where θ'_Δ is the rate threshold.

$$\phi_n - \phi_{n-k} = \frac{1}{N} \sum_{i=1}^{N} \left(\theta_{n,i} - \theta_{n-k,i}\right), \quad N = 9, k = l \text{ or } 2. \quad (5)$$

The initial pointing system motion symbol Mod.C_n can be expressed as

$$\text{Mod} \cdot C_n = \text{Sign}\,(\psi_n, \psi_{n-k}, \theta'_\Delta)$$

$$= \begin{cases} +, & \psi_n - \psi_{n-k} \geq \theta'_\Delta \,(\text{Positive}), \\ 0, & \text{Others}\,(\text{Stop}, k = l \text{ or } 2), \\ -, & \psi_n - \psi_{n-k} \leq -\theta'_\Delta \,(\text{Reverse}), \end{cases} \quad (6)$$

$$\psi_n - \psi_{n-k} = \frac{1}{N} \sum_{i=1}^{N} \left(\theta_{n,i} - \theta_{n-k,i}\right), \quad N = 9, k = l \text{ or } 2. \quad (7)$$

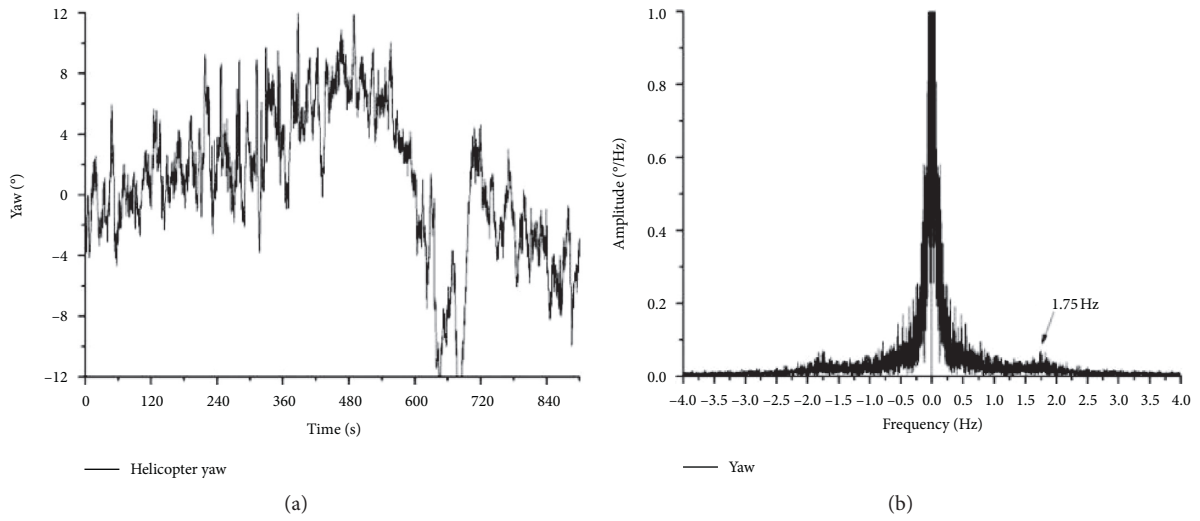The tracking symbol Mod.D_n can be expressed as

(a)

(b)

FIGURE 15: (a) Azimuth change of helicopter hovering. (b) Azimuth spectrum change of helicopter hovering.
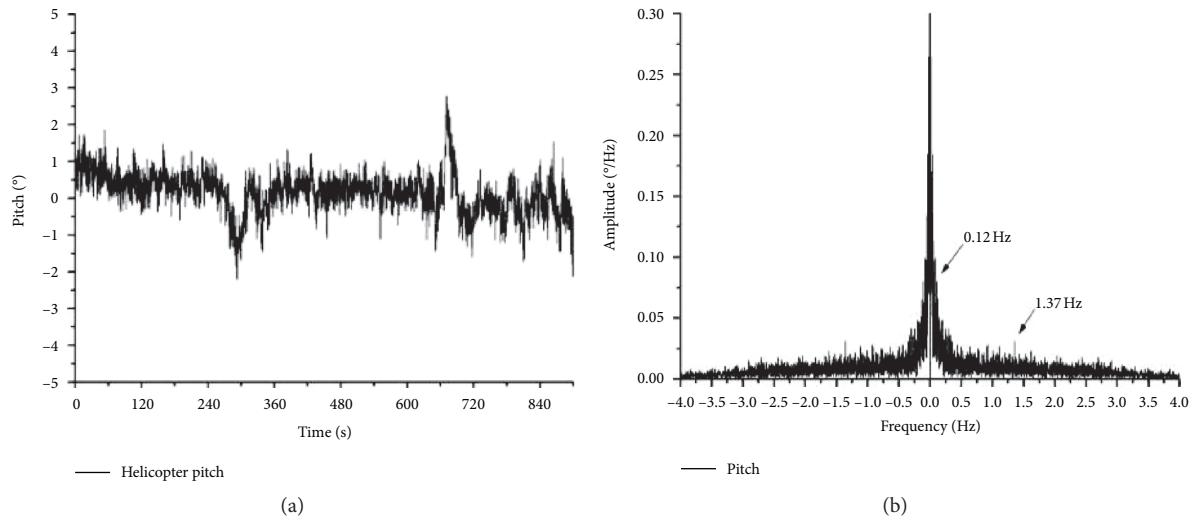

(a)

(b)

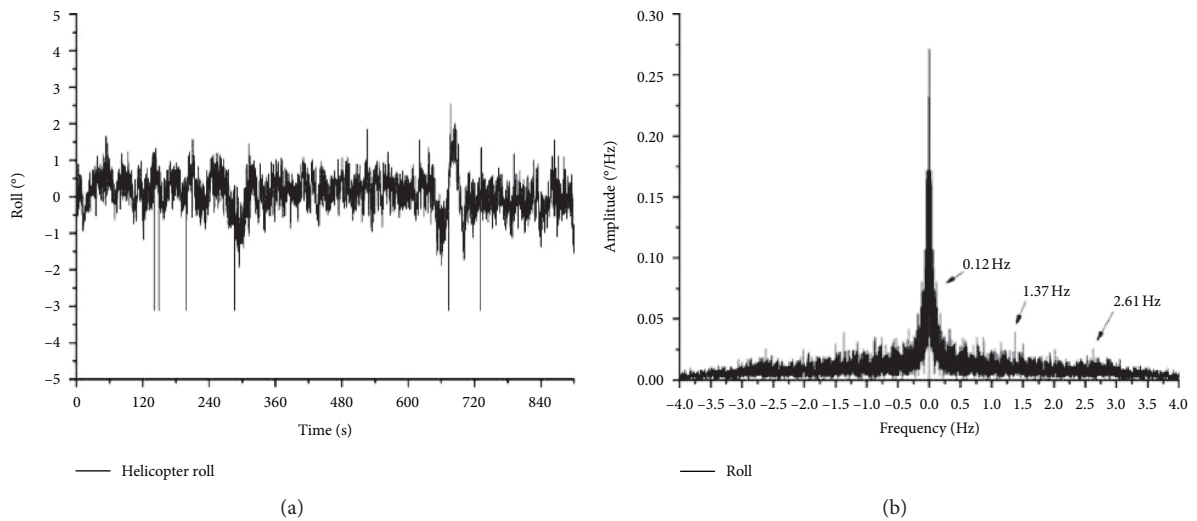FIGURE 16: (a) Pitch angle change of helicopter hovering. (b) Pitch spectrum change of helicopter hovering.

(a)

(b)

FIGURE 17: (a) Roll angle change of helicopter hovering. (b) Rollover spectrum change of helicopter hovering.

$$\text{Mod.}D_n = \text{Sign}\left(\psi_n - \psi_{n-k}, \phi_n - \phi_{n-k}, \theta_\Delta''\right)$$

$$= \begin{cases} +, & \text{abs}\left(\psi_n - \psi_{n-k}\right) - \text{abs}\left(\phi_n - \phi_{n-k}\right) \geq \theta_\Delta'' \text{ (Faster than)}, \\ 0, & \text{Others (Same speed, } k = l \text{ or 2)}, \\ -, & \text{abs}\left(\psi_n - \psi_{n-k}\right) - \text{abs}\left(\phi_n - \phi_{n-k}\right) \leq -\theta_\Delta'' \text{ (Slower than)}, \end{cases} \tag{8}$$

where θ_Δ' is the rate difference threshold.

The symbol vector in the identity control can be expressed as

$$\text{Mod}_n = \left[\text{Mod.}D_n, \text{Mod.}C_n, \text{Mod.}B_n, \text{Mod.}A_n\right]. \tag{9}$$

In the control process, the clockwise direction is "forward" and the counterclockwise direction is "reverse." In the control strategy, "●"—turntable rate remains unchanged; "○"—turntable has no pulse output; "−"—the turntable is reversed and the speed is constant; "+"—turntable is positive. "−↑"—reverse acceleration of turntable; "−↓"—reverse deceleration of turntable; "+↑"—turntable forward acceleration; "+↓"—turntable forward deceleration; "+●"—the forward rate of the turntable is unchanged; "−●"—the reverse rate of the turntable is unchanged; and "X"—turntable is an abnormal state that requires reacquisition data judgment.

In the tracking process of Figure 19, at the $T_{n+1} \longrightarrow T_{n+7}$ time, the target is stationary in the forward direction of the turntable. At the $T_{n+7} \longrightarrow T_{n+15}$ time, the target moves at a constant speed in the forward direction. At the beginning of phase T_{n-1}, the turntable is at rest. The control vector $\begin{bmatrix} 0 & 0 & 0 & - \end{bmatrix}$ at this time can be obtained according to formulas (2), (4), (6), and (8). Then, the output pulse F_{n-1} is given, and the pulse value is evenly output within the control interval. At time T_n, it is judged that the control vector is $\begin{bmatrix} + & + & 0 & - \end{bmatrix}$, and the control strategy that should be performed at this time is "+●."

It is just starting to track, the tracking strategy is corrected to "+↑," giving the output pulse F_n and speeding up the tracking. At each subsequent time, the judgment and output process repeats the abovementioned parts and finally achieves the purpose of tracking the target [18, 19].

4.2. Dichotomy Control Parameter Update. In the initial direction tracking process, the corresponding control strategy is generated after the control vector is quickly calculated and acquired in real time. The core of the control strategy is to generate the appropriate amount of control. In this system, the number F_n of output pulses of the stepping motor is the controlled amount. By changing it, the tracking motion of the stepping motor at the set speed can be realized. Under different control strategies, the value F_n is updated according to the dichotomy [18]. The principle of the dichotomy is to increase or decrease the value of the controlled parameter by one-half of the nonzero change value before the controlled parameter, thereby achieving the goal of quickly tracking the target. The dichotomy substitution formula can be expressed as

$$F_n = \begin{cases} (\text{Update.Direct}). \min\left\{\text{abs}\left(F_n\right) + (\text{Update.Speed}).2^{-1}.\text{abs}\left[\text{abs}\left(F_n - 1\right) - \text{abs}\left(F_m\right)\right], F_{\text{Max}}\right\}, \\ (\text{Update.Direct}). \max\left\{\text{abs}\left(F_n\right) + (\text{Update.Speed}).2^{-1}.\text{abs}\left[\text{abs}\left(F_n - 1\right) - \text{abs}\left(F_m\right)\right], F_{\text{Min}}\right\}. \end{cases} \tag{10}$$

Among them, F_{max} is the maximum number of pulses, and F_{min} is the minimum number of pulses. F_m is the value of the first absolute value not equal to F_{n-1} before the time $n-1$. Updata.Direct is the update direction operator and Updata.Speed is the update speed operator. Among them, the calculation process of the update operator is as follows:

$$\text{Updata.Direct} = \begin{cases} +1, & \text{" + ",} \\ \pm 0, & \text{"o",} \\ -1, & \text{" − ",} \end{cases} \tag{11}$$

$$\text{Updata.Speed} = \begin{cases} +1, & \text{"↑",} \\ 0, & \text{"●",} \\ -1, & \text{"↓".} \end{cases} \tag{12}$$

The control strategy can be processed according to equations (10) to (12) to obtain the updated pulse value.

4.3. Overshoot and Advance Compensation. In the initial pointing system, since the load on the turntable has 150 kg, the moment of inertia is huge. In the process of acceleration, deceleration, and reversing, the inertia overshoot phenomenon will inevitably occur in the turntable. This overshoot can cause instability during the tracking process. However, due to the existence of the turbine and the worm structure, the inertia moment caused by the inertia of the load is equivalent to the motor shaft, which is already small. Generally, the motor's out-of-step problem can be ignored when the motor is working within the working torque range.

When tracking a moving target with uniform velocity, there is a time lag between the target sample and the motor output, which makes the turntable always have a time lag error in the tracking process. Set the advance compensation amount F_Δ under a specific control strategy and correct formula (10). Then, this lag error can be compensated, and the correction formula is
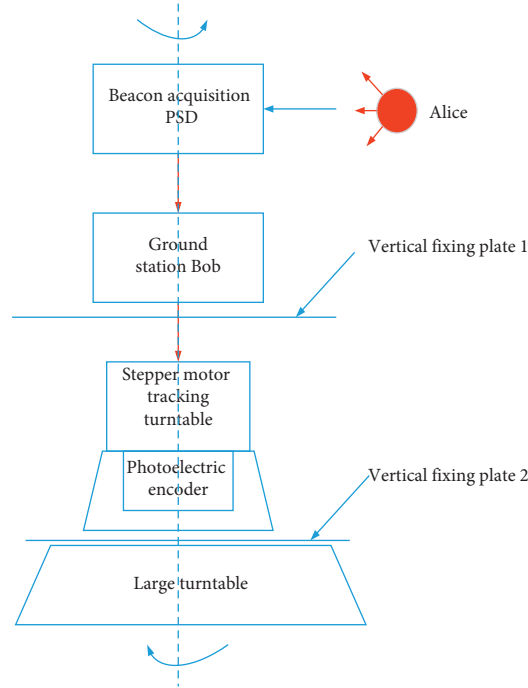
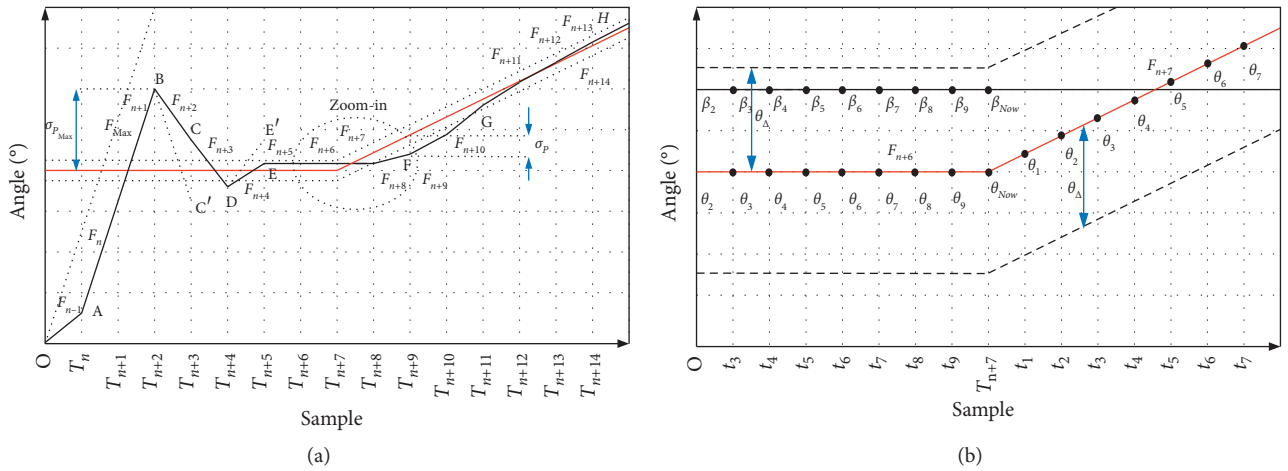FIGURE 18: Initial pointing system of ground station Bob.

(a)

(b)

FIGURE 19: Identification tracking control method. (a) Identification control method. (b) Target and tracking value sampling.

$$F_n = \begin{cases} (1).\min\{\mathrm{abs}(F_n) + (2).2^{-1}.\mathrm{abs}[\mathrm{abs}(F_n - 1) - \mathrm{abs}(F_m)] + (2).F\Delta, F_{\mathrm{Max}}\}, \\ (1).\max\{\mathrm{abs}(F_n) + (2).2^{-1}.\mathrm{abs}[\mathrm{abs}(F_n - 1) - \mathrm{abs}(F_m)] + (2).F\Delta, F_{\mathrm{Min}}\}, \end{cases} \tag{13}$$

$$(1) = (\mathrm{Updata.Direct}). \ (2) = (\mathrm{Updata.Speed}).$$

5. Control Performance and Effect

The control strategy, which is based on the identification method, can be regarded as a special structure that introduces expert control (symbol vector) in the traditional PID control method.

Comparing with the traditional PI control and PID control, the method has the following characteristics: the

overshoot of the control output is small; the dynamic and static characteristics are stable, and the parameters can be adaptively adjusted. Here is an example of a type I controlled object [20, 21]. The transfer function of the controlled object is

$$G_0 = \frac{1}{s(s + 1)(s + 5)}. \tag{14}$$

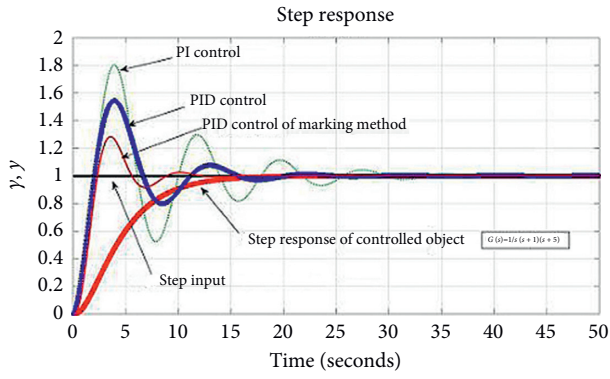FIGURE 20: Comparison of control effects.

FIGURE 21: Initial pointing tracking experiment.

FIGURE 22: Tracking effect when 1°/s triangle wave input.

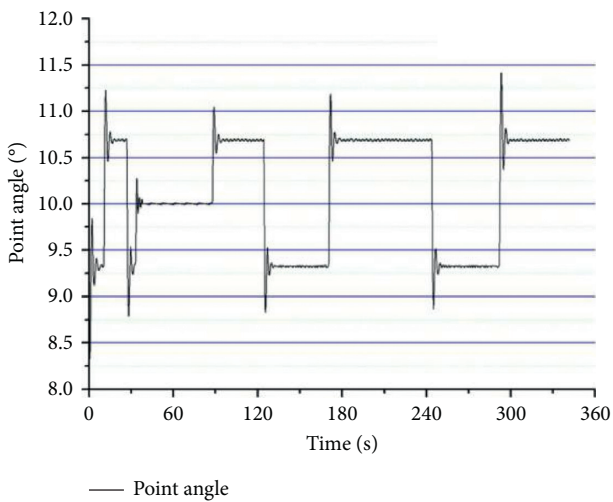FIGURE 23: Tracking effect at 0.5°/s triangle wave input.
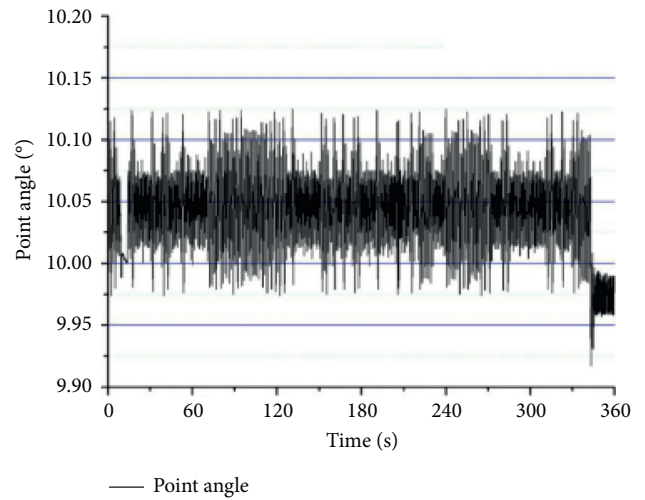
FIGURE 24: Tracking effect at 0.1°/s triangle wave input.

The open-loop transfer function of the PID controller is

$$G_c = K_p + \frac{K_i}{s} + K_d. \tag{15}$$

For the controlled object represented by formula (14), the Ziegler–Nichols empirical tuning formula can be used to know that the PI tuning factor ($K_p = 13.5$ and $K_i = 5.79$) and PID tuning coefficient of the above system is ($K_p = 18, K_i = 12.9,$ and $K_d = 6.3$). Then, the step response curve of the above-controlled
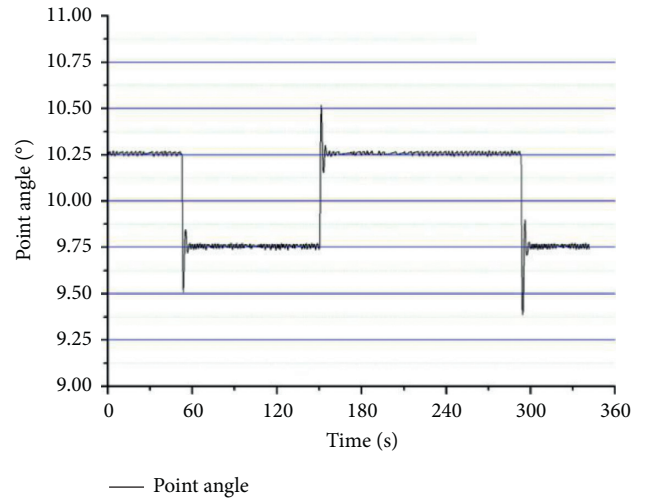
object under the conventional PI control, PID control, and identification method control strategy are as shown in Figure 20.

The actual lab test environment for the initial pointing system is shown in Figure 21.

In Figure 21, the simulation of the target motion is performed using a 2 m mesa high-precision large turntable produced by Kunming Machine Tool Plant. The simulated speed and initial pointing control results are shown in the following figure, and the tracking target is 10°. The tracking results are shown in Figures 22–24.

(1) When the large turntable is input with a triangular wave of 1°/s, the initial pointing tracking curve is as shown in Figure 23.

As can be seen from Figure 22, the parameters are as follows: tracking deviation <0.7°, tracking speed 1°/s, and tracking fluctuation <0.1°.

(2) When the large turntable is input with a 0.5°/s triangular wave, the initial pointing tracking curve is as shown in Figure 23.

As can be seen from Figure 24, the parameters are as follows: tracking deviation <0.25°, tracking speed 0.5°/s, and tracking fluctuation <0.1°.

(3) When the large turntable is input with a 0.1°/s triangular wave, the initial pointing tracking curve is shown in Figure 24.

It can be seen from Figure 24, the parameters are as follows: tracking deviation <0.1°, tracking speed 0.1°/s, and tracking fluctuation <0.1°.

6. Conclusion

In the quantum key distribution (QKD) technology test, to verify the ground motion platform, this paper carried out field tests on different motion platforms. By analyzing the motion characteristics of the vehicle motion platform, the hot-air balloon floating motion platform, and the airborne motion platform, the parameters and spectrum components of different motion platforms are obtained. In the frequency domain, by decomposing the frequency of the motion platform, an inertial damping platform is added to its motion characteristics, thereby isolating the high-frequency vibration of the motion platform itself is achieved. By establishing the symbol vector, a tracking control strategy based on the symbol method is proposed. The disadvantages of modification of the control parameters in the conventional PID control are greatly improved, and the stability and adaptability of the tracking control process are increased. The control strategy table of the identification method is established to realize the tracking control process of the stepping motor. The control parameters of the ATP tracking system are optimized, and the experimental work in the free-space quantum key distribution is completed.

Data Availability

The data used to support the findings of this study are available from the corresponding author upon request.

Conflicts of Interest

The authors declare that they have no conflicts of interest regarding the publication of this paper.

Acknowledgments

References

[1] M. Rajan and S. M. Jagjit, "An innovative approach for performance enhancement of 320 Gbps free space optical communication system over turbulent channel," *Optical and Quantum Electronics*, vol. 51, no. 9, p. 289, 2019.

[2] J. J. Wu, J. Ma, L. Y. Tan, and S. Y. Yu, "Condition for keeping polarization invariant on propagation in space-to-ground optical communication downlink," *Optics Communications*, vol. 453, Article ID 124410, 2019.

[3] C. W. Fei, H. T. Liu, Z. Z. Zhu et al., "Whole-process design and experimental validation of landing gear lower drag stay with global/local linked driven optimization strategy," *Chinese Journal of Aeronautics*, 2020.

[4] R. Afnan, G. Salman, and A. Rizwan, "Integration of millimeter-wave and optical link for duplex transmission of hierarchically modulated signal over a single carrier and fiber for future 5G communication systems," *Telecommunication Systems*, vol. 72, no. 2, pp. 221–229, 2019.

[5] P. Marin-Palomo, J. N. Kemal, M. Karpov et al., "Microresonator-based solitons for massively parallel coherent optical communications," *Nature*, vol. 546, no. 7657, pp. 274–279, 2017.

[6] L. Tan, Q. Yang, S. Yu et al., "Statistical distribution of fiber-coupling efficiency in the satellite-to-ground downlink," *Optical Engineering*, vol. 50, no. 10, Article ID 105001, 2011.

[7] A. Banerjee, S. Mandal, P. Roy et al., "A compact scintillator based position sensitive detector system for gamma ray tracking applications," *Nuclear Instruments and Methods in Physics Research Section A: Accelerators, Spectrometers, Detectors and Associated Equipment*, vol. 930, pp. 100–104, 2019.

[8] C. W. Fei, H. T. Liu, S. L. Li et al., "Dynamic parametric modeling-based model updating strategy of aero-engine casings," *Chinese Journal of Aeronautics*, pp. 1–13, 2021.

[9] L. Han, C. Chen, T. Guo et al., "Probability-based service safety life prediction approach of raw and treated turbine blades regarding combined cycle fatigue," *Aerospace Science and Technology*, vol. 110, no. 3, Article ID 106513, 2021.

[10] H. Liu, W. Song, M. Li, A. Kudreyko, and E. Zio, "Fractional Lévy stable motion: finite difference iterative forecasting model," *Chaos, Solitons & Fractals*, vol. 133, no. 4, Article ID 109632, 2020.

[11] H. T. Gao, "Development of foreign Earth observation satellite technology," *Spacecraft Engineering*, vol. 18, no. 3, pp. 84–92, 2009.

[12] J.-Y. Lin and Y.-C. Liao, "Small-angle measurement with highly sensitive total-internal-reflection heterodyne interferometer," *Applied Optics*, vol. 53, no. 9, pp. 1903–1908, 2014.

[13] Z. Ding, G. Sun, M. Guo et al., "Effect of phase transition on micro-grinding-induced residual stress," *Journal of Materials Processing Technology*, vol. 281, Article ID 116647, 2020.

[14] W. Guo, C. Wu, Z. Ding, and Q. Zhou, "Prediction of surface roughness based on a hybrid feature selection method and long short-term memory network in grinding," *The International Journal of Advanced Manufacturing Technology*, vol. 112, no. 9-10, pp. 2853–2871, 2021.

[15] Z. Huang, X. Zhang, X. Li et al., "Defect model of domain nucleation growth induced by interlayer in poly (vinylidene fluoride-trifluoroethylene) ultrathin films," *Journal of Physics D: Applied Physics*, vol. 54, no. 13, 2020.

[16] T. Wang, "Symbol stability analysis of uncertain systems with convex polyhedron," *Control Theory & Applications*, vol. 32, no. 1, pp. 35–42, 2015.

[17] H. Liu, W. Song, Y. Niu, and E. Zio, "A generalized Cauchy method for remaining useful life prediction of wind turbine gearboxes," *Mechanical Systems and Signal Processing*, vol. 153, no. 15, Article ID 107471, 2021.

[18] Y. Gao, F. Villecco, M. Li, and W. Song, "Multi-scale permutation entropy based on improved LMD and HMM for rolling bearing diagnosis," *Entropy*, vol. 19, no. 4, p. 176, 2017.

[19] X. Han and W. Zhou, "Optimal threshold of error decision related to non-uniform phase distribution QAM signals generated from MZM based on OCS," *Optics Communications*, vol. 410, no. 1, pp. 623–626, 2018.

[20] V. A. Oliveira, L. V. Cossi, M. C. M. Teixeira, and A. M. F. Silva, "Synthesis of PID controllers for a class of time delay systems," *Automatica*, vol. 45, no. 7, p. 1778, 2009.

[21] H. Liu, W. Song, and E. Zio, "Generalized Cauchy difference iterative forecasting model for wind speed based on fractal time series, forecasting model for wind speed based on fractal time series," *Nonlinear Dynamics*, vol. 103, no. 1, pp. 1–15, 2021.